O_2- and α-Ketoglutarate-Dependent Tyrosyl Radical Formation in TauD, an α-Keto Acid-Dependent Non-Heme Iron Dioxygenase†

Matthew J. Ryle,‡,§ Aimin Liu,∥,# Rajendra Bose Muthukumaran,⊥ Raymond Y. N. Ho,∥ Kevin D. Koehntop,∥ John McCracken,⊥ Lawrence Que, Jr.,∥ and Robert P. Hausinger*,‡,§

Departments of Microbiology and Molecular Genetics, Biochemistry and Molecular Biology, and Chemistry, Michigan State University, East Lansing, Michigan 48824, and Department of Chemistry and Center for Metals in Biocatalysis, University of Minnesota, Minneapolis, Minnesota 55455

Received September 11, 2002; Revised Manuscript Received December 18, 2002

ABSTRACT: Taurine/α-ketoglutarate dioxygenase (TauD), a non-heme mononuclear Fe(II) oxygenase, liberates sulfite from taurine in a reaction that requires the oxidative decarboxylation of α-ketoglutarate (αKG). The lilac-colored αKG-Fe(II)TauD complex (λ_{max} = 530 nm; ϵ_{530} = 140 $M^{-1}\cdot cm^{-1}$) reacts with O_2 in the absence of added taurine to generate a transient yellow species (λ_{max} = 408 nm, minimum of 1600 $M^{-1}\cdot cm^{-1}$), with apparent first-order rate constants for formation and decay of ∼0.25 s^{-1} and ∼0.5 min^{-1}, that transforms to yield a greenish brown chromophore (λ_{max} = 550 nm, 700 $M^{-1}\cdot cm^{-1}$). The latter feature exhibits resonance Raman vibrations consistent with an Fe(III) catecholate species presumed to arise from enzymatic self-hydroxylation of a tyrosine residue. Significantly, ^{18}O labeling studies reveal that the added oxygen atom derives from solvent rather than from O_2. The transient yellow species, identified as a tyrosyl radical on the basis of EPR studies, is formed after αKG decomposition. Substitution of two active site tyrosine residues (Tyr73 and Tyr256) by site-directed mutagenesis identified Tyr73 as the likely site of formation of both the tyrosyl radical and the catechol-associated chromophore. The involvement of the tyrosyl radical in catalysis is excluded on the basis of the observed activity of the enzyme variants. We suggest that the Fe(IV) oxo species generally proposed (but not yet observed) as an intermediate for this family of enzymes reacts with Tyr73 when substrate is absent to generate Fe(III) hydroxide (capable of exchanging with solvent) and the tyrosyl radical, with the latter species participating in a multistep TauD self-hydroxylation reaction.

Enzymes in the α-ketoglutarate (αKG)[1] dioxygenase superfamily contain mononuclear Fe(II) active sites and catalyze a diverse range of chemical transformations that are often, but not always, coupled to the oxidative decarboxylation of αKG (*1*−*3*). Clavaminic acid synthase (CS) typifies the chemical versatility of this enzyme class; it performs hydroxylation, oxidative cyclization, and desaturation reactions during synthesis of the *β*-lactamase inhibitor clavulanic acid (*4*). More commonly, members of this enzyme family catalyze specific hydroxylations of protein side chains, plant metabolites, or other compounds (*5*). Proposed chemical mechanisms by which these mononuclear sites catalyze their reactions commonly invoke a high-valent iron−oxo species (*6*−*8*) by analogy to the mechanisms associated with heme enzymes, but direct evidence for such a species is not yet available.

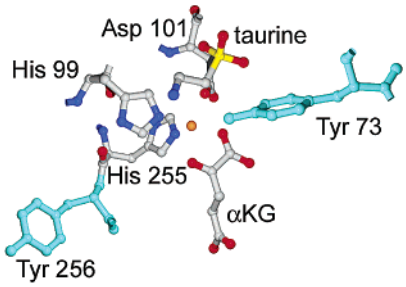

FIGURE 1: TauD active site. The structure of taurine-αKG-Fe(II)-TauD (*10*) reveals the amino acid ligands to the metallocenter (His99, Asp101, and His255), the binding locations of αKG and taurine cosubstrates, and the positions of two tyrosine residues (Tyr73 and Tyr256) found within 10 Å of the metal center.

Here, we focus on one representative of the αKG-dependent dioxygenase superfamily, taurine (2-aminoethanesulfonate)/αKG dioxygenase or TauD. This *Escherichia coli* enzyme is synthesized in response to sulfur starvation and allows cells to utilize this widely available sulfur donor by converting it to sulfite and aminoacetaldehyde (see Scheme 1) (*9*). The initial steps in TauD catalysis are reasonably well understood. Fe(II) binds reversibly to His99, Asp101, and

† These studies were supported by the National Institutes of Health (Postdoctoral Fellowship GM20196 to M.J.R. and Grants GM063584 to R.P.H., GM33162 to L.Q., and GM54065 to J.M.).

* To whom correspondence should be addressed. Tel: 517-355-6463 ext 1610. Fax: 517-353-8957. E-mail: hausinge@msu.edu.

‡ Department of Microbiology and Molecular Genetics, Michigan State University.

§ Department of Biochemistry and Molecular Biology, Michigan State University.

∥ University of Minnesota.

Current address: Department of Biohemistry, University of Mississippi Medical Center.

⊥ Department of Chemistry, Michigan State University.

[1] Abbreviations: αKG, α-ketoglutarate; CS, clavaminate synthase; DAOCS, deacetoxycephalosporin C synthase; dopa, dihydroxyphenylalanine; EPR, electron paramagnetic resonance; TauD, taurine/αKG dioxygenase; TfdA, 2,4-dichlorophenoxyacetate/αKG dioxygenase.

10.1021/bi026832m CCC: $25.00
Published on Web 01/31/2003

Scheme 1

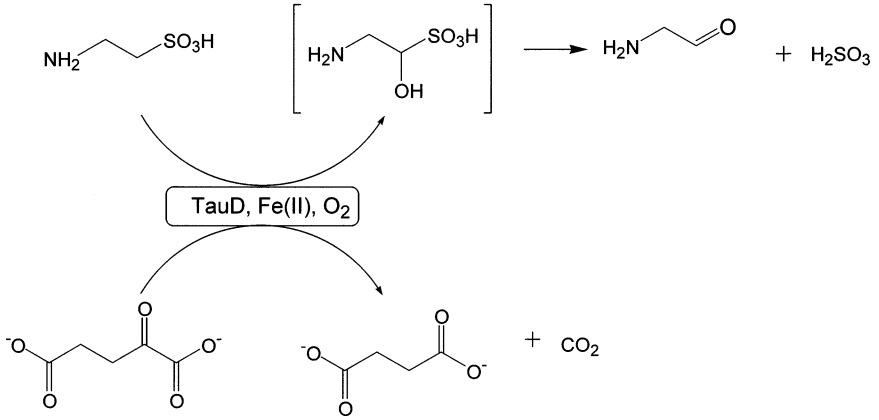

His255 on the basis of X-ray crystallographic characterization of TauD (Figure 1) (*10*) and site-directed mutagenesis studies of the closely related enzyme TfdA [2,4-dichlorophenoxyacetate (2,4-D)/αKG dioxygenase] (*11*). Three water molecules likely occupy the remaining cis-oriented sites of the substrate-free TauD octahedral center by analogy to the Fe(II)-bound waters observed in the crystal structure of deacetoxycephalosporin C synthase (DAOCS), an enzyme involved in the synthesis of cepham-based antibiotics (*12*). Binding of αKG to Fe(II)TauD results in the bidentate coordination of the C-1 carboxyl and C-2 carbonyl oxygens on the basis of TauD structural analysis (Figure 1) (*10*) as well as on electronic (*13*) and resonance Raman (*14*) characterization of the binary TauD complex, magnetic circular dichroism studies of αKG-Fe(II)CS (*15*), and structures of the αKG-bound forms of Fe(II)CS, Fe(II)-DAOCS, and Fe(II) anthocyanidin synthase (*4*, *12*, *16*). Structural elucidation of taurine-αKG-Fe(II)TauD (Figure 1) (*10*) combined with spectroscopic studies of TauD (*13*, *14*) and CS (*17*, *18*) indicate that substrate does not bind directly to the metal but that its binding to the anaerobic αKG-Fe(II)-enzyme complex displaces the remaining solvent molecule to create an O_2 binding site. Subsequent steps involving reaction of oxygen with the ternary complex remain unclear.

Investigation of αKG-Fe(II)TauD reactivity toward oxygen revealed a novel self-hydroxylation reaction, as presented below. Significantly, evidence for the participation of a tyrosyl radical in this TauD modification was obtained.

EXPERIMENTAL PROCEDURES

Enzyme Purification and Assay. Wild-type TauD apoprotein was purified and assayed as previously described (*13*). Selected variants of TauD, described below, were purified and assayed in the same manner. The activities of wild-type and variant TauD proteins were observed to decrease over the assay time course; thus, progress curves were analyzed by fitting the data to the equation

$$P_t = V_i(1 - e^{-k(\text{inact})t})k(\text{inact})^{-1} \quad (1)$$

where P_t is the accumulated product at time t, V_i is the initial velocity, and k(inact) is the inactivation rate constant (*19*).

Site-Directed Mutants of TauD Lacking Active Site Tyrosines. The Y73I, Y73S, Y256I, and Y256F variants of TauD were created by direct mutation of *tauD* in pME4141 (*9*) by using the Stratagene Quickchange System (Stratagene, La Jolla, CA). The mutagenic primers used were (Y256I) 5′-CGCGTGACCCAGCACATTGCCAATGCCGATTAC-3′, (Y256F) 5′-CGCGTGACCCAGCACTTTGCCAATGC-CGATTAC-3′, (Y73I) 5′-GAATTGATTCACCCTGTTAT-TCCGCATGCCGAAGGG-3′, and (Y73S) 5′-GAATT-GATTCACCCTGTTAGCCCGCATGCCGAAGGG-3′. The mutated plasmids were subcloned into DH5α (Invitrogen, Carlsbad, CA) and purified by using a Wizard Midi-Prep Kit (Promega, Madison, WI), and the identities were confirmed by sequence analysis.

Spectroscopy. Stopped-flow UV/visible spectra were obtained by using a 0.4 cm path length Olis RSM-16 UV/visible stopped-flow spectrophotometer as previously described (*13*). Additional electronic spectra were recorded on a Beckman DU 7500 spectrophotometer in a 1 cm path length cuvette. Resonance Raman spectra were collected on an Acton AM-506 spectrometer (1200-groove grating) using a Kaiser Optical holographic supernotch filter and a Princeton Instruments liquid N_2-cooled (LN-1100PB) CCD detector with 4 cm^{-1} spectral resolution. The 647.1 and 568.2 nm laser excitation lines at 100 mW power were obtained with a Spectra Physics BeamLok 2060-KR-V krypton ion laser. The Raman spectra were obtained at room temperature by 90° scattering in a spinning cell, and Raman frequencies were referenced to indene. For each sample the entire spectral range was obtained by collecting spectra at two different frequency windows, and the resulting spectra were spliced together. Baseline corrections (polynomial fits) and curve fits (Gaussian functions) were carried out by using Grams/32 Spectral Notebase version 4.04 (Galactic). EPR spectra were recorded on a Bruker ESP300E spectrometer equipped with an Oxford liquid He cryostat.

HPLC Methods. Quantitation of the concentration of αKG remaining and succinate produced during O_2 treatment was carried out by using HPLC methods. Samples of Fe(II)TauD (0.5 mM in subunit and metal ions) were adjusted to 1 mM αKG, and the headspace was exchanged to 100% O_2 while the extent of chromophore formation was monitored. Alternatively, sample containing 0.55 mM subunit, 0.5 mM Fe(II), and 2 mM αKG was mixed with an equal volume of O_2-saturated buffer, and the extent of chromophore formation was monitored. Aliquots (100 μL) were removed at selected time points for HPLC determination, and the reactions were quenched by the addition of 5 μL of 6 M H_2SO_4. The samples were centrifuged for 5 min, and 50 μL aliquots were loaded

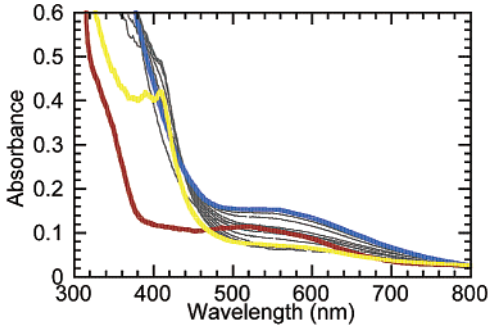

FIGURE 2: Repetitive scan UV/visible spectroscopic analysis of the reaction of αKG-Fe(II)TauD with oxygen-saturated buffer. Spectra were obtained for anaerobic Fe(II)TauD (0.5 mM ferrous ammonium sulfate and 0.55 mM TauD subunit in 25 mM Tris buffer, pH 8.0) containing 2 mM αKG (red trace) and the sample 13 s after adding an equal volume of O_2-saturated buffer (yellow trace) or longer times up to 100 min (gray traces) in a cuvette of 1 cm path length. In addition, a scan was taken after 3 h (blue trace).

onto an Aminex HPX-87H column (Bio-Rad) using a Shimadzu LC-10AD VP pump equipped with a Waters universal LC injector (Model U6K). The organic acids were eluted using 0.013 M H_2SO_4 and detected by a Waters differential refractometer (Model R401). Data were plotted on a HP 3390A integrator and the concentrations determined by comparison to solutions of known concentration.

RESULTS

Reaction of αKG-Fe(II)TauD with O_2. Upon being mixed with buffer equilibrated under 100% O_2, the lilac-colored chromophore associated with anaerobic αKG-Fe(II)TauD (λ_{max} = 530 nm; ϵ_{530} = 140 $M^{-1}\cdot cm^{-1}$) converted initially to a yellow species (λ_{max} = 408 nm; minimum ϵ_{408} = 1600 $M^{-1}\cdot cm^{-1}$) that slowly transformed to a greenish brown chromophore (λ_{max} = 550 nm; ϵ_{550} = 460 $M^{-1}\cdot cm^{-1}$) as shown in Figure 2. Significantly, the 408 nm species was not observed during oxygen exposure of taurine-αKG-Fe(II)-TauD or αKG-free Fe(II)TauD. Furthermore, the presence of αKG and the absence of taurine were required for formation of the 550 nm species. The intensities of the transient and 550 nm chromophores were highly dependent on the concentration of Fe(II). Maximal 408 nm chromophore formation was observed when Fe(II) concentrations were approximately stoichiometric with the subunit concentrations.

The production of the two chromophores in O_2-exposed αKG-Fe(II)TauD is reminiscent of, but distinct from, the generation of a blue species (ϵ_{580} = 1000 $M^{-1}\cdot cm^{-1}$) observed in the uncoupled reaction of O_2 with αKG-Fe(II)-TfdA (*20*). The TfdA-derived spectrum arises from self-hydroxylation of Trp112 (located adjacent to the His113 metal ligand), ligand exchange, and metal oxidation to form an Fe(III)-O-Trp chromophore. The TauD results suggest that a unique self-hydroxylation reaction may take place in this protein. Because resonance Raman spectroscopic characterization was critical to the identification of the TfdA chromophore, analogous spectroscopic studies were carried out with TauD.

Resonance Raman Spectroscopy of O_2-Exposed αKG-Fe(II)TauD. The resonance Raman spectrum of the greenish brown sample derived from exposure of αKG-Fe(II)TauD to O_2 exhibits a set of vibrations not observed in the spectrum of αKG-Fe(II)TauD before exposure to O_2 (Figure 3). This

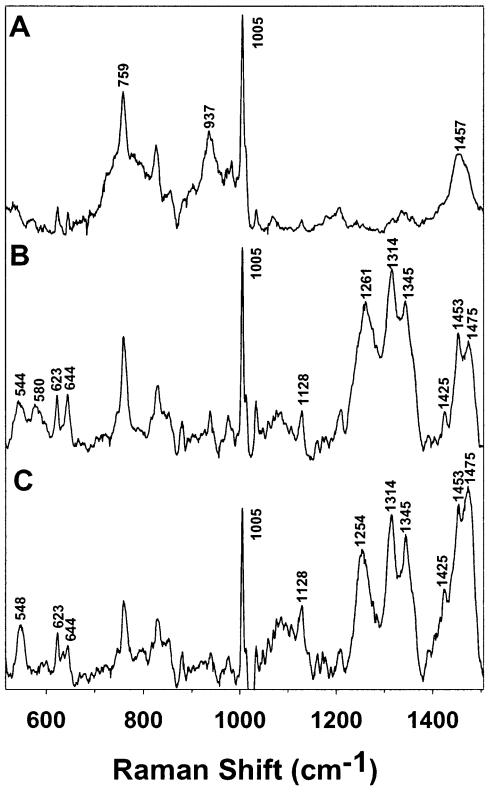

FIGURE 3: Resonance Raman spectrum of αKG-TauD species. Raman spectra were obtained for the (A) lilac-colored αKG-Fe(II)-TauD (568.2 nm excitation), (B) a greenish brown sample formed upon exposure of αKG-Fe(II)TauD to O_2 (647.1 nm excitation), and (C) a greenish brown sample formed upon exposure of αKG-Fe(II)TauD in $H_2{}^{18}O$ to O_2 (647.1 nm excitation).

spectrum resembles those of tyrosine hydroxylase complexed with various catecholamines (*21*, *22*) and those of recombinant phosphomannose isomerase and the R2 protein of ribonucleotide reductase obtained from an F208Y mutation (Table 1), both of which possess dihydroxyphenylalanine (dopa) side chains chelated to the metal center (*23*, *24*). Specifically, the bands in the 1100−1500 cm^{-1} region arise from catecholate ring deformations, while those at 500−650 cm^{-1} can be assigned to metal−ligand vibrations associated with the five-membered iron−catecholate chelate ring. In contrast, the pattern of peak frequencies and intensities in the TauD spectrum is distinctly different from those of protocatechuate 3,4-dioxygenase (*25*), uteroferrin (*26*), and O_2-exposed αKG-Fe(II)TfdA (*20*), respectively ruling out the presence of Fe(III)-O-Tyr and Fe(III)-O-Trp chromophores. Thus it would appear that a tyrosine residue has become hydroxylated to dopa in the course of forming the greenish brown chromophore.

Isotope labeling experiments have been carried out to determine the origin of the oxygen atom that is inserted into the Tyr residue. Samples were prepared from αKG-Fe(II)-TauD in $H_2{}^{16}O$ buffer and exposed to $^{18}O_2$ or from αKG-Fe(II)TauD in $H_2{}^{18}O$ buffer and exposed to $^{16}O_2$ (Figure 3C). The 1261 cm^{-1} band is associated with an aromatic ring deformation involving the catecholate C−O bonds (*22*). No shift is observed in the $^{18}O_2$ experiment, but there is a 7 cm^{-1} downshift in the $H_2{}^{18}O$ experiment. For comparison, a 4 cm^{-1} downshift is reported for the tyrosine hydroxylase-[3-^{18}O]-dopamine complex (*22*), but no shift is observed for [3-^{18}O]-dopa208 R2 (*23*). While the reason for this variability is not

Table 1: Resonance Raman Vibrations of Proteins with Fe(III) Catecholate and Related Chromophores

protein/complex[a]	Raman vibrations (cm^{-1})												ref
αKG-Fe(II)TauD + O_2	544	580	623	644	1128	1261	1314	1345	1425	1453	1475		this work
αKG-Fe(II)TauD + $^{18}O_2$	?	?	623	644		1261	1314	1345	1425	1453	1475		
αKG-Fe(II)TauD + O_2 in $H_2{}^{18}O$	548		623	644	1128	1254	1314	1345	1425	1453	1475		
dopa208 RNR R2	512	592	619		1143	1263	1319	1350			1475	1569	*23*
[3-^{18}O]dopa208 RNR R2	499	584	617		1143	1263	1319	1350			1475	1569	
TH-dopamine	528	592	631			1275	1320		1425		1475		*22*
TH-[3-^{18}O]dopamine	522	580	629			1271	1320		1425		1475		
TH-noradrenaline	530	624	636		1171	1271	1328		1428		1476		*22*
TH-[3-^{18}O,4-^{18}O]noradrenaline	512	552−597	624		1168	1266	1317		1424		1474		
recombinant phosphomannose isomerase		591	631			1266	1330		1428		1482	1650	*24*
protocatechuate 3,4-dioxygenase (Fe-O-Tyr)		592		826 854	1172 1180	1254 1266					1506	1604	*26*
uteroferrin (Fe-O-Tyr)		575		805 872	1168	1285					1503	1603	*27*
αKG-Fe(II)TfdA + O_2 (Fe-O-Trp)		564	750	898 970	1240	1274	1344					1622	*20*

[a] RNR R2 = the R2 protein of ribonucleotide reductase from *E. coli*; TH = tyrosine hydroxylase.

apparent, it is clear that ^{18}O from water, but not from O_2, is incorporated into the newly formed catecholate of TauD.

Unfortunately, interpretation of the isotope effects in the low-frequency region is not as straightforward. The two sharper features at 623 and 644 cm^{-1}, both assigned to the Fe−O4 vibration, are unaffected in the isotope labeling experiments (Table 1). This is not surprising as O4 is the native oxygen atom of the Tyr residue that is converted to dopa. The fact that there are two features associated with Fe−O4 is attributed to the presence of two forms of the enzyme, respectively with and without the bound bicarbonate derived from the oxidative decarboxylation of αKG. Expulsion of the bound bicarbonate by addition of the substrate taurine results in the loss of the 623 cm^{-1} peak.[2] The Fe−O3 stretch is associated with the much broader feature at 580 cm^{-1} in the ^{16}O enzyme. This band disappears upon the incorporation of ^{18}O from water into the catecholate (Figure 3C). In isotope labeling studies of other protein complexes with dopa-like ligands, the vibration associated with the Fe−O3 bond has been observed to downshift upon ^{18}O incorporation into the 3-O atom (Table 1). However, rationalizing the disappearance of the 580 cm^{-1} band in the TauD spectrum would require a rather large downshift of ca. 35 cm^{-1} so that it merges with the 544 cm^{-1} feature. Furthermore, corresponding spectra from the $^{18}O_2$ experiments are difficult to interpret because the features below 600 cm^{-1} appear even broader. Despite the ambiguity of the low-frequency data, the accumulated results nevertheless indicate that the dopa O3 oxygen atom in TauD derives from water, just like the oxygen atom incorporated into the HO-Trp residue formed upon exposure of αKG-Fe(II)TfdA to O_2 (*20*).

Stopped-Flow Spectroscopic Analysis of the 408 nm Intermediate in O_2-Exposed αKG-Fe(II)TauD. To better define the properties of the transient 408 nm species, stopped-flow UV/visible spectroscopic methods were used. This analysis allowed examination of the kinetics of formation of the 408 nm feature (and the accompanying 385 nm shoulder) generated upon mixing αKG-Fe(II)TauD with 100% O_2-saturated buffer (Figure 4). Enzyme, αKG, Fe(II), and oxygen were all required to obtain this yellow species. As summarized in Table 2, the rate constant for 408 nm species formation (∼0.25 s^{-1}) was independent of the concentrations of iron and αKG but did appear to depend on oxygen concentration. Not surprisingly, the signal amplitudes were diminished in cases where the αKG or oxygen concentrations were less than that of the enzyme subunit. When measured over the first 20 min, this feature decayed in an apparent first-order process at 0.58 ± 0.10 min^{-1} and then declined an additional ∼15% over the next 2 h.

Table 2: Effect of Reactant Concentration on the Rate of 408 nm Chromophore Formation

[αKG] (mM)	[Fe(II)] (mM)	[TauD] (mM)	[O_2] (mM)	obsd rate (s^{-1})[a]	amplitude	ns[b]	np[c]
0.125	0.25	0.275	0.5	0.20 ± 0.03	0.072	12	3
0.25	0.25	0.275	0.5	0.20 ± 0.02	0.113	8	2
0.5	0.25	0.275	0.5	0.22 ± 0.01	0.143	3	1
1.0	0.25	0.275	0.5	0.21 ± 0.01	0.134	6	2
2.0	0.25	0.275	0.5	0.27 ± 0.04	0.114	10	4
4.0	0.25	0.275	0.5	0.22 ± 0.03	0.113	15	3
4.0	0.125	0.275	0.5	0.23 ± 0.04	0.068	11	3
4.0	0. 25	0.275	0.1	0.11 ± 0.03	0.052	8	3

[a] Rates were obtained by using a single-wavelength, single-exponential fitting routine provided in the Olis software package. Individual scans were fit from 10 ms to 15 s. [b] Number of stopped-flow traces averaged to obtain the presented rates. [c] Number of independent protein preparations used for comparisons.

EPR Spectroscopic Changes in O_2-Exposed αKG-Fe(II)-TauD. The transient yellow chromophore described above exhibited features reminiscent of those reported previously for tyrosyl radicals (*27*, *28*); hence, confirmatory studies were carried out using electron paramagnetic resonance (EPR) spectroscopy to test for such a species. Oxygen exposure of αKG-Fe(II)TauD led to the rapid development of an intense EPR feature at $g = 2$ in addition to a rhombic high-spin Fe(III) signal at $g = 4.3$ (Figure 5A). Comparison to a 1,1-diphenyl-2-picrylhydrazyl standard of known concentration suggested stoichiometric formation (0.9 ± 0.4 spin per mole of subunit) of this radical species, again in a process requiring enzyme, αKG, Fe(II), and oxygen. Expanded spectra of the $g = 2$ feature recorded at 4, 100, and 220 K (Figure 5B) highlight the effect of temperature on the signal line shape. Simulation of the spectrum recorded at 165 K (Figure 5C) was achieved by using *g*-values and proton hyperfine

[2] M. J. Ryle, K. D. Koehntop, A. Liu, L. Que, Jr., and R. P. Hausinger, unpublished observations.

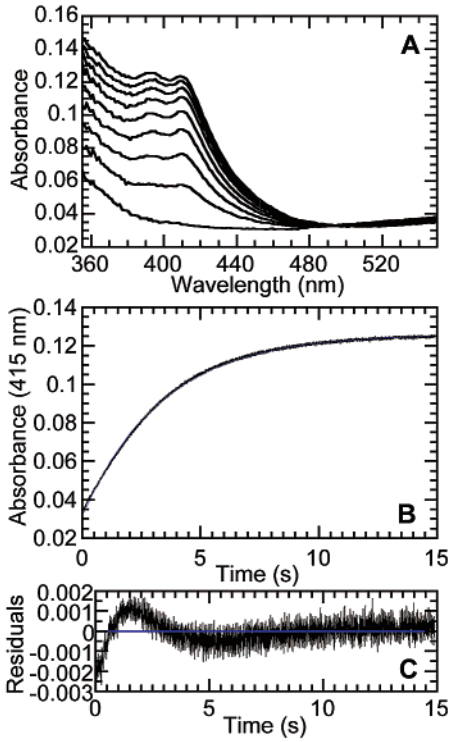

FIGURE 4: Formation of the transient yellow intermediate during reaction of αKG-Fe(II)TauD with oxygen using stopped-flow UV/visible spectroscopy. (A) Stopped-flow spectral changes were analyzed upon mixing equal volumes of 100% O_2-saturated buffer and αKG-Fe(II)TauD (1.0 mM αKG, 0.55 mM TauD subunit, and 0.5 mM ferrous ammonium sulfate) in 25 mM Tris buffer, pH 8.0. The least intense spectrum was recorded at 10 ms, and spectra with increasing intensity were obtained at 1 s intervals (0.4 cm path length). (B) A single-exponential fit of the observed changes in 408 nm absorbance over time yielded a rate constant of chromophore formation of 0.29 ± 0.02 s^{-1}. The plot includes both the data and the overlapping fit. (C) The residuals are shown for the single-exponential fit.

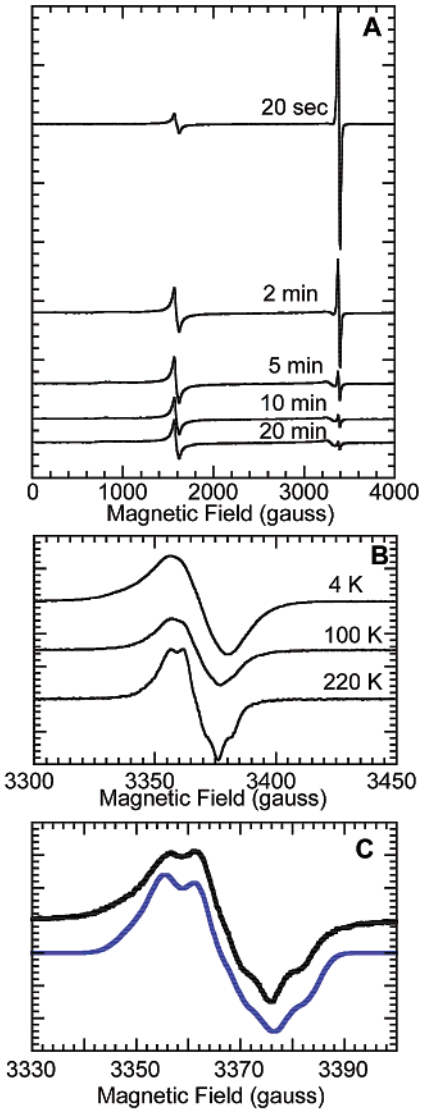

FIGURE 5: EPR spectroscopic evidence for a transient tyrosyl radical in TauD. (A) The EPR spectra recorded at 4 K using 50 μW microwave power for samples frozen at the indicated times after mixing equal volumes of αKG-Fe(II)TauD (2 mM αKG, 0.5 mM ferrous ammonium sulfate, and 0.6 mM protein subunit) and O_2-saturated buffer. A single-exponential fit (not shown) of the change in peak-to-peak intensity of the $g = 2$ signal (using values at 3375.2 and 3398.5 G) versus time resulted in a rate of signal loss of 0.50 ± 0.02 min^{-1}. (B) Expanded spectra of the $g = 2.0$ region recorded at 4, 100, and 200 K for the O_2-exposed (~13 s) sample containing 0.5 mM αKG, 0.25 mM ferrous ammonium sulfate, and 0.28 mM TauD subunit. (C) Simulation (blue trace) and experimental spectrum (black trace) for an analogous sample recorded at 165 K. The simulation provided the following spin Hamiltonian parameters: g_x, 2.0068; g_y, 2.0044; g_z, 2.0023; proton hyperfine coupling constants (in MHz), methylene protons (24.5, 24, 31) and (<6, <6, <6); 2,6 protons (−7.0, −4.4, −1.1); 3,5 protons (−27.3, −8.8, −19.6).

coupling constants consistent with those previously reported for tyrosyl radicals (see figure caption for magnetic resonance parameter values) (*27*−*29*). These proton hyperfine couplings predict an odd-alternate distribution of the unpaired electron spin density about the aromatic ring as well as dihedral angles of 48° and 72° for the orientation of the methylene protons relative to the ring plane (*30*). The EPR signal attributed to the tyrosyl radical decayed over time at room temperature (Figure 5A), coincident with loss of the 408 nm species.

To address the question of proximity of the tyrosyl radical to the high-spin Fe center, inversion recovery experiments using the three-pulse spin−echo sequence ($\pi - T - \pi/2 -$ tau$-\pi-$tau−echo) were carried out. In these experiments, the amplitude of the spin−echo was monitored as a function of T, keeping tau in the spin−echo sequence constant. Data obtained at 5 K show complex recovery functions that can be fit to a single-exponential decay with a lifetime of 11 μs. This estimate of T_1 is about 1000 times shorter than that measured by Evelo et al. (*31*) for the dark-stable tyrosyl radical of photosystem II at 5 K. In that system, relaxation was enhanced by the Mn cluster of the oxygen-evolving apparatus that is approximately 15−20 Å away (*32*). Because the dipolar contribution to the spin−lattice relaxation varies as $S(S + 1)/r^6$, we would expect to gain a factor of 10 in recovery rate based on the higher spin of the Fe center. However, the additional factor of 100 in T_1 enhancement likely results from a dipolar distance that is a factor of 2 shorter. On the basis of these preliminary results, the metal center is likely 7−10 Å from the tyrosyl radical. As shown in Figure 1, both Tyr73 and Tyr256 residues are within this distance of the metal center. Experiments to assess the effects of spectral and spin diffusion on our measured T_1 values are currently underway.

Temporal Relationships among αKG Decomposition, Spectroscopic Changes, and Enzyme Inactivation. The head-

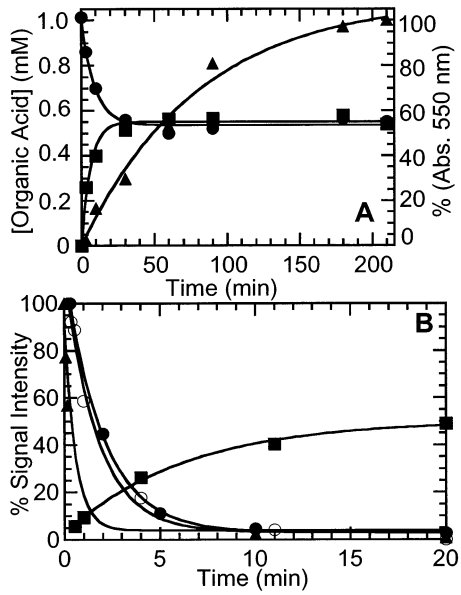

FIGURE 6: Relationships among αKG consumption, succinate formation, and chromophore formation during O_2 treatment of αKG-Fe(II)TauD. (A) Anaerobic samples of Fe(II)TauD (0.5 mM in subunit and metal ions) were adjusted to 1 mM αKG and exposed to 100% O_2 without shaking while the extent of chromophore formation was monitored (triangles). Aliquots were removed for HPLC determination of αKG (circles) and succinate (squares) at the indicated times. (B) An analogous sample was mixed with 100% O_2-saturated buffer. The changes in spectral intensities at 550 nm (squares) and 408 nm (open circles) were each fit to single-exponential processes for data collected between 25 s to 20 min, resulting in rates of 0.18 ± 0.04 min^{-1} and 0.58 ± 0.10 min^{-1}. Also shown is the remaining activity (triangles) and the $g = 2$ EPR signal intensity (closed circles, derived from Figure 7A) fitted to rates of 1.7 ± 0.7 min^{-1} and 0.50 ± 0.02 min^{-1}, respectively.

space of a vial containing anaerobic αKG-Fe(II)TauD was replaced by 100% O_2 while changes in the organic acid concentrations and 550 nm absorption were monitored (Figure 6A). This method of mixing the sample with oxygen resulted in a slow absorption increase at 550 nm compared to that observed by mixing sample with oxygen-saturated buffer (Figure 2 or 6B) but allowed greater ease in monitoring the levels of αKG and succinate. Chromophore formation occurred after the consumption of approximately 1 equiv of αKG and generation of about 1 equiv of succinate per TauD subunit. When the reaction was repeated by mixing the anaerobic sample with an equal volume of O_2-saturated buffer, the chromophore (Figure 6B, squares) formed at a greatly increased rate (0.18 ± 0.04 min^{-1} using data collected up to 20 min), and nearly stoichiometric levels (0.8 per subunit) of the organic acid were converted to succinate and CO_2 within 0.2 min (not shown). Incubation for a total of 100 min led to a doubling of the intensity of the 550 nm absorption (to the 100% value in Figure 6B) and the decomposition of an additional 0.4 αKG per subunit. Significantly, the tyrosyl radical formed rapidly and decayed (monitored by the decrease in 408 nm absorption and by loss of EPR spectral intensity with first-order rate constants of 0.58 ± 0.10 min^{-1} and 0.50 ± 0.02 min^{-1}, respectively) prior to generation of the 550 nm species.

The activity of the αKG-Fe(II)TauD sample was assessed at different times after mixing with oxygen. Anaerobic solutions of αKG-Fe(II)TauD were mixed with equal volumes of O_2-saturated buffer [resulting in final concentrations

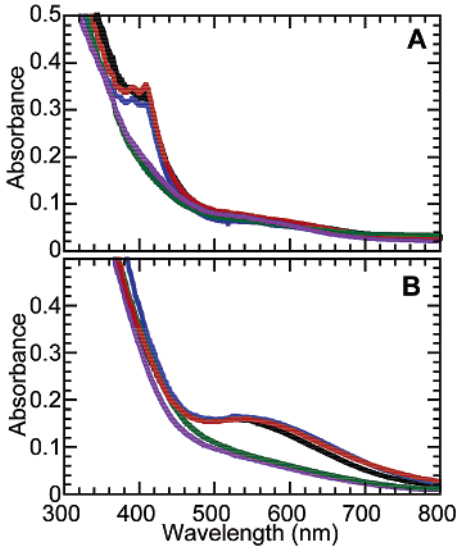

FIGURE 7: UV/visible spectroscopic analysis of the reaction of αKG-bound TauD variants with oxygen. Spectra were obtained ~10 s (A) and 2 h (B) after mixing anaerobic αKG-Fe(II)TauD samples (0.5 mM ferrous ammonium sulfate, 0.55 mM TauD subunit, and 2 mM αKG in 25 mM Tris buffer, pH 8.0) with equal volumes of O_2-saturated buffer. Spectra are presented for wild-type TauD (black trace) and the Y256I (blue trace), Y256F (red trace), Y73I (green trace), and Y73S (purple trace) variants.

of 275 μM TauD subunit, 250 μM Fe(II), and 0.5 mM αKG] for varied periods of time, adjusted to 250 μM taurine, further reacted for 1 min, quenched by EDTA addition, and analyzed for sulfite. As shown in Figure 6B (triangles), taurine additions at 5, 10, 60, 600, and 1200 s resulted in the production of 170, 125, 63, 5.4, and 2.0 μM sulfite. For comparison, a control sample with taurine present in the original solution yielded 220 μM sulfite. Thus, as shown in Figure 6B, the enzyme lost activity more rapidly (1.7 min^{-1}) than the observed decay of the tyrosyl radical. This result is not surprising when one considers that, in addition to any irreversible inactivation that may occur from side chain modification, TauD is likely to be reversibly inactivated simply by oxidation of the metal center on the basis of studies carried out with TfdA (*19*). Indeed, ~60% of the original TauD activity was recovered by dithionite reduction, EDTA treatment, dialysis, and reintroduction to the assay conditions.

Properties of TauD Variants. Enzyme variants were created with substitutions at Tyr73 and Tyr256 (located 6.5 and 9.3 Å from the metallocenter, respectively; Figure 1) to assess the possibility that an active site tyrosine residue is modified in the reaction of αKG-Fe(II)TauD with oxygen. As shown in Figure 7, formation of the tyrosyl radical (observed at 408 nm) required the presence of Tyr73 but not Tyr256. Furthermore, the greenish brown chromophore was clearly formed in the Tyr256 mutant proteins, but the variants lacking Tyr73 exhibited significantly reduced absorbance at 550 nm with no clear maximum. These results suggest that Tyr73 participates in the formation of both of these chromophores. Analysis of TauD variants confirmed that Tyr73 was required to generate the EPR signal signifying radical formation (Figure 8).

To assess the potential importance of Tyr73 and Tyr256 to catalysis, the kinetic properties of the Y73I, Y73S, Y256I, and Y256F TauD variants were compared to the activity of the wild-type enzyme (Figure 9 and Table 3). Significantly,

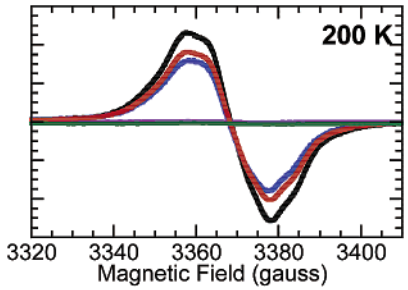

FIGURE 8: EPR spectroscopic analysis of the reaction of αKG-bound TauD variants with oxygen. Anaerobic αKG-Fe(II)TauD (0.5 mM ferrous ammonium sulfate, 0.55 mM TauD subunit, and 2 mM αKG in 25 mM Tris buffer, pH 8.0) was mixed with an equal volume of O_2-saturated buffer. Spectra are presented for wild-type TauD (black trace) and the Y256I (blue trace), Y256F (red trace), Y73I (green trace), and Y73S (purple trace) variants. Samples were frozen at ~13 s, and the EPR spectra were recorded at 200 K using 50 μW microwave power.

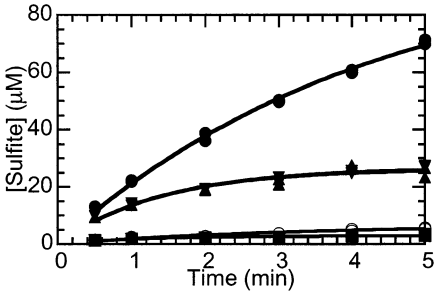

FIGURE 9: Progress curves of wild-type and mutant TauD proteins. The production of sulfite (*9*) was monitored as a function of time using standard assay conditions in the presence of 640 μM taurine. Samples examined included 1 μg of wild-type TauD (closed circles) or 2 μg of the Y73I (inverted closed triangles), Y256F (closed triangles), Y73S (open circles), and Y256 I (closed squares) variants.

Table 3: Summary of Kinetic Parameters for Wild-Type TauD and Selected Variants

enzyme	K_M (taurine) (μM)	k_{cat} (min^{-1})	k_{cat}/K_M ($\mu M^{-1} min^{-1}$)	inactivation rate[a] (min^{-1})
wild type	58 ± 6	758 ± 26	13.1 ± 1.8	0.19 ± 0.04
Y73I	243 ± 33	438 ± 35	1.80 ± 0.32	0.76 ± 0.06
Y256F	122 ± 17	371 ± 16	3.04 ± 0.55	0.52 ± 0.07

[a] Calculated for data using 1 mM taurine.

each of these modified proteins was active, thus establishing that neither of these tyrosines is essential for catalysis. Although past studies had assumed linear kinetics over the first few minutes of the assay (*9*, *13*), the TauD variants and, to a lesser extent, the wild-type enzyme exhibited inactivation kinetics within this time frame (Figure 9). This behavior is not surprising since the activities of several αKG-dependent dioxygenases are known to decrease over time in a process that is partially reversed by ascorbic acid. For example, the related enzyme TfdA was shown to undergo a combination of irreversible inactivation (possibly associated with enzyme self-hydroxylation (*20*)) and ascorbate-reversible inactivation (presumably due to metal oxidation) (*19*). TauD was inactivated 35% more rapidly in the absence of ascorbate (k_{inact} 0.25 ± 0.04 min^{-1}) than in its presence (Table 3) when compared at 1 mM taurine. On the basis of the calculated initial rates shown in Table 3, each of the mutant proteins is less active than the wild-type enzyme (detailed kinetics are provided for only two variants since the other two mutant proteins exhibited very little activity). Some loss of activity is not unexpected for cases where active site residues are altered, as demonstrated by prior studies with TfdA (*33*). In particular, Tyr73 has been suggested to participate in binding taurine via a hydrogen-bonding interaction (*10*). Consistent with this assignment, the Y73I mutant protein resulted in a 5-fold increase in K_M of taurine compared to the wild-type enzyme. In contrast, a more modest 2-fold increase in K_M was observed for the Y256F variant.

DISCUSSION

We have obtained evidence demonstrating that αKG-Fe(II)TauD reacts with oxygen in the absence of taurine to generate a transient tyrosyl radical that subsequently gives rise to a catechol. This self-hydroxylation reaction is manifested by the appearance of a greenish brown chromophore that arises from a catecholate-to-iron(III) charge-transfer transition (λ_{max} 550 nm, ϵ 700 $M^{-1}\cdot cm^{-1}$). Compared with other iron(III) catecholate chromophores such as those found in the complexes of tyrosine hydroxylase with dopamine or noradrenaline (*22*), dopa208 R2 (*34*), and recombinant phosphomannose isomerase (*24*), greenish brown TauD has an extinction coefficient that is about one-third as large, suggesting that only ~33% of the enzyme has been modified. This assessment is consistent with the observation that about 60% of enzyme activity can be recovered after treating samples with a reducing agent plus chelator, dialyzing, and examining the enzyme in fresh assay buffer. On the basis of results from site-directed mutagenesis studies, we identified Tyr73 as the site of both radical and catechol formation. Below, we discuss a reasonable chemical mechanism to account for these transformations. In addition, we relate these results to uncoupled reactions observed in the broader family of non-heme oxygenases and speculate on the possible roles of these transformations.

The multistep sequence of reactions described above for oxygen-exposed αKG-Fe(II)TauD appears to be initiated with O_2-dependent αKG decomposition. This reaction is likely to parallel that which occurs during catalysis in the presence of taurine. In the commonly invoked mechanism for this enzyme family (Scheme 2), an iron(IV) oxo species responsible for substrate oxidation is suggested to be derived from O_2 binding to the iron(II) αKG center and attack by the bound superoxide on the α-keto carbon of αKG, followed by decarboxylation and heterolytic O−O bond cleavage (*4*, *6*−*8*). There is currently no direct spectroscopic evidence for this iron(IV) oxo intermediate, although such species have been observed for heme (*35*) and for non-heme diiron enzymes such as methane monooxygenase (*36*) and ribonucleotide reductase (*27*). Perhaps this lack of evidence speaks to the relative instability and greater reactivity of a mononuclear iron(IV) oxo species in a non-heme ligand environment. We propose that when substrate is absent, the TauD iron−oxo species still forms but attacks the nearby (6.5 Å distant) Tyr73 instead, leading to formation of the tyrosyl radical and an Fe(III) OH center. The transient tyrosyl radical in TauD then rebounds with the Fe(III) OH center to form an iron(II) catecholate complex. Subsequent oxidation in the presence of air generates the observed 550 nm chromophore. It is clear from the kinetic data presented above that the Tyr·/Fe(III) OH intermediate must have a sufficient lifetime to allow solvent exchange to occur with the

Scheme 2

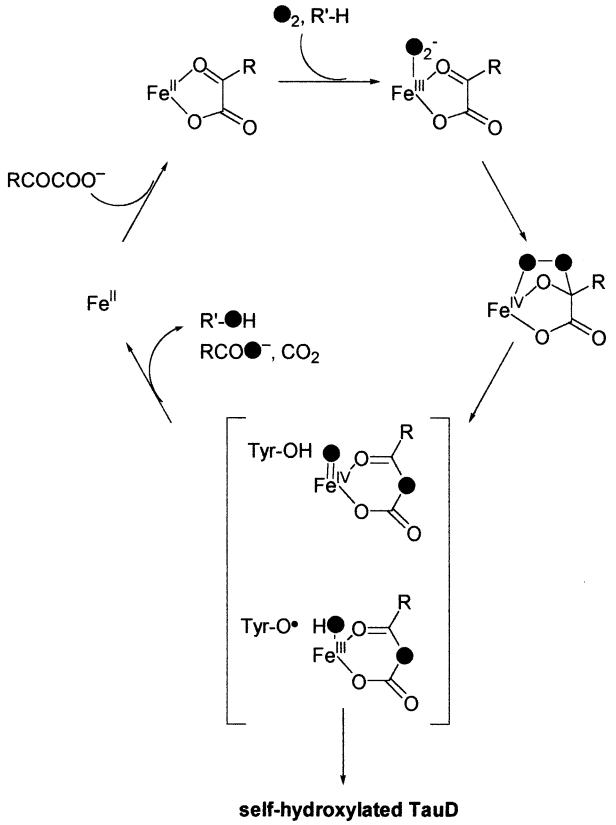

kinetically labile high-spin Fe(III) center, thereby providing a mechanism for the incorporation of ^{18}O from $H_2{}^{18}O$ into the resulting dopa residue as detected in the resonance Raman studies. A similar mechanism is proposed for the formation of the dopa residue in dopa208 R2 with the 3-O atom derived from solvent water (*23*). In this case, the Fe to Tyr distance is 5.3 Å (*27*).

The αKG-dependent dioxygenases are known to exhibit low, but detectable, oxygen reactivity in the presence of only αKG and metal ions (e.g., refs *13* and *20*). In contrast, binding of the primary substrate leads to increased oxygen reactivity due to displacement of a water molecule from the six-coordinate αKG-bound active site, thus creating a binding site for O_2 (e.g., refs *13*, *17*, and *18*). It has long been known that the αKG-dependent dioxygenases undergo oxidative inactivation in the presence of poor substrates due to the uncoupling of αKG decomposition and substrate oxidation (e.g., refs *37*−*40*). As observed here with TauD, ascorbate can enhance the activity of these enzymes by reducing the oxidized metallocenter to restore the catalytically active Fe(II) state. In addition to this reversible type of inactivation, irreversible modifications of these proteins also occur (*19*). For example, oxygen exposure of αKG-Fe(II)TfdA results in hydroxylation of an active site Trp residue (*20*), and oxidation of 1-aminocyclopropane-1-carboxylate oxidase leads to enzyme fragmentation (*41*). The results described here provide another example of irreversible modifications due to oxidative reactions involving tyrosine. On the basis of the rapid inactivation of our Tyr73 variants, we speculate that tyrosine hydroxylation may afford protection to TauD by preventing more damaging reactivity (e.g., backbone cleavage) with activated oxygen intermediates. More significantly, these studies provide the first evidence related to the identity of a distinct intermediate, a tyrosyl radical, in the oxidative inactivation of any αKG-dependent dioxygenase. The likely involvement of a tyrosyl radical in TauD self-hydroxylation reactions may relate to the mechanisms of tyrosine or tryptophan amino acid side chain hydroxylation or cross-linking reactions noted in selected other non-heme iron and other metal-containing proteins (*27*). These modifications, including the hydroxy-Trp in TfdA (*20*) and F208Y hydroxylation in the R2 protein of ribonucleotide reductase (*42*), likely form through the participation of aromatic radical intermediates.

In conclusion, we suggest that oxygen-exposed αKG-Fe(II)TauD catalyzes oxidative decomposition of the α-keto acid analogous to that occurring during catalysis when taurine is present, resulting in generation of a putative, formally iron(IV) oxo species. We further suggest that this moiety reacts with the nearby Tyr73 to form an iron(III) amino acid radical species, as depicted in Scheme 2. The TauD radical species then participates in additional reactions resulting in the catechol-containing derivative.

ACKNOWLEDGMENT

This paper is dedicated to the memory of Gerald T. Babcock, a pioneer in investigations of tyrosyl radicals. We thank Will and Joan Broderick for insightful discussions and Greta Monterosso for assistance with selected studies.

REFERENCES

1. Prescott, A. G., and Lloyd, M. D. (2000) The iron(II) and 2-oxoacid-dependent dioxygenases and their role in metabolism, *Nat. Prod. Rep. 17*, 367−383.
2. Schofield, C. J., and Zhang, Z. (1999) Structural and mechanistic studies on 2-oxoglutarate-dependent oxygenases and related enzymes, *Curr. Opin. Struct. Biol. 9*, 722−731.
3. Ryle, M. J., and Hausinger, R. P. (2002) Non-heme iron oxygenases, *Curr. Opin. Chem. Biol. 6*, 193−201.
4. Zhang, Z., Ren, J., Stammers, D. K., Baldwin, J. E., Harlos, K., and Schofield, C. J. (2000) Structural origins of the selectivity of the trifunctional oxygenase clavaminic acid synthase, *Nat. Struct. Biol. 7*, 127−133.
5. Prescott, A. G., and John, P. (1996) Dioxygenases: molecular structure and role in plant metabolism, *Annu. Rev. Plant Physiol. Plant Mol. Biol. 47*, 245−271.
6. Hanauske-Abel, H. M., and Gunzler, V. (1982) A stereochemical concept for the catalytic mechanism of prolylhydroxylase. Applicability to classification and design of inhibitors, *J. Theor. Biol. 94*, 421−455.
7. Que, L., Jr., and Ho, R. Y. N. (1996) Dioxygen activation by enzymes with mononuclear non-heme iron active site, *Chem. Rev. 96*, 2607−2624.
8. Solomon, E. I., Brunold, T. C., Davis, M. I., Kemsley, J. N., Lee, S.-K., Lehnert, N., Neese, F., Skulan, A. J., Yang, Y.-S., and Zhou, J. (2000) Geometric and electronic structure/function correlations in non-heme iron enzymes, *Chem. Rev. 100*, 235−349.
9. Eichhorn, E., van der Ploeg, J. R., Kertesz, M. A., and Leisinger, T. (1997) Characterization of α-ketoglutarate-dependent taurine dioxygenase from *Escherichia coli*, *J. Biol. Chem. 272*, 23031−23036.
10. Elkins, J. M., Ryle, M. J., Clifton, I. J., Dunning Hotopp, J. C., Lloyd, J. S., Burzlaff, N. I., Baldwin, J. E., Hausinger, R. P., and Roach, P. L. (2002) X-ray crystal structure of *Escherichia coli* taurine/α-ketoglutarate dioxygenase complexed to ferrous iron and substrates, *Biochemistry 41*, 5185−5192.
11. Hogan, D. A., Smith, S. R., Saari, E. A., McCracken, J., and Hausinger, R. P. (2000) Site-directed mutagenesis of 2,4-dichlorophenoxyacetic acid/α-ketoglutarate dioxygenase. Identification of residues involved in metallocenter formation and substrate binding, *J. Biol. Chem. 275*, 12400−12409.
12. Valegård, K., Terwisscha van Scheltinga, A. C., Lloyd, M. D., Hara, T., Ramaswamy, S., Perrakis, A., Thompson, A., Lee, W.-J., Baldwin, J. E., Schofield, C. J., Hajdu, J., and Andersson, I.

(1998) Structure of a cephalosporin synthase, *Nature* (*London*) *394*, 805−809.
13. Ryle, M. J., Padmakumar, R., and Hausinger, R. P. (1999) Stopped-flow kinetic analysis of *Escherichia coli* taurine/α-ketoglutarate dioxygenase: interactions with α-ketoglutarate, taurine, and oxygen, *Biochemistry 38*, 15278−15286.
14. Ho, R. Y. N., Mehn, M. P., Hegg, E. L., Liu, A., Ryle, M. A., Hausinger, R. P., and Que, L., Jr. (2001) Resonance Raman studies of the iron(II)-α-keto acid chromophore in model and enzyme complexes, *J. Am. Chem. Soc. 123*, 5022−5029.
15. Pavel, E. G., Zhou, J., Busby, R. W., Gunsior, M., Townsend, C. A., and Solomon, E. I. (1998) Circular dichroism and magnetic circular dichroism spectroscopic studies of the non-heme ferrous active site in clavaminate synthase and its interaction with α-ketoglutarate cosubstrate, *J. Am. Chem. Soc. 120*, 743−753.
16. Wilmouth, R. C., Turnbull, J. J., Welford, R. W. D., Clifton, I. J., and Schofield, C. J. (2002) Structure and mechanism of anthocyanadin synthase from *Arabidopsis thaliana*, *Structure 10*, 93−103.
17. Zhou, J., Gunsior, M., Bachmann, B. O., Townsend, C. A., and Solomon, E. I. (1998) Substrate binding to the α-ketoglutarate-dependent non-heme iron enzyme clavaminate synthase 2: coupling mechanism of oxidative decarboxylation and hydroxylation, *J. Am. Chem. Soc. 120*, 13539−13540.
18. Zhou, J., Kelly, W. L., Bachmann, B. O., Gunsior, M., Townsend, C. A., and Solomon, E. I. (2001) Spectroscopic studies of substrate interactions with clavaminate synthase 2, a multifunctional α-KG-dependent non-heme iron enzyme: correlation with mechanisms and reactivities, *J. Am. Chem. Soc. 123*, 7388−7398.
19. Saari, R. E., and Hausinger, R. P. (1998) Ascorbic acid-dependent turnover and reactivation of 2,4-dichlorophenoxyacetic acid/α-ketoglutarate dioxygenase using thiophenoxyacetic acid, *Biochemistry 37*, 3035−3042.
20. Liu, A., Ho, R. Y. N., Que, L., Jr., Ryle, M. J., Phinney, B. S., and Hausinger, R. P. (2001) Alternative reactivity of an α-ketoglutarate-dependent iron(II) oxygenase: enzyme self-hydroxylation, *J. Am. Chem. Soc. 123*, 5126−5127.
21. Andersson, K. K., Cox, D. D., Que, L., Jr., Flatmark, T., and Haavik, J. (1988) Resonance Raman studies on the blue-green-colored bovine adrenal tyrosine 3-monooxygenase (tyrosine hydroxylase). Evidence that the feedback inhibitors adrenaline and noradrenaline are coordinated to iron, *J. Biol. Chem. 263*, 18621−18626.
22. Michaud-Soret, I., Andersson, K. K., Que, L., Jr., and Haavik, J. (1995) Resonance Raman studies of catecholate and phenolate complexes of recombinant human tyrosine hydroxylase, *Biochemistry 34*, 5504−5510.
23. Ling, J., Sahlin, M., Sjöberg, B.-M., Loehr, T. M., and Sanders-Loehr, J. (1994) Dioxygen is the source of the μ-oxo bridge in iron ribonucleotide reductase, *J. Biol. Chem. 269*, 5595−5601.
24. Smith, J. J., Thomson, A. J., Proudfoot, A. E. I., and Wells, T. N. C. (1997) Identification of an Fe(III)-dihydroxyphenylalanine site in recombinant phosphomannose isomerase from *Candida albicans*, *Eur. J. Biochem. 244*, 325−333.
25. Siu, D. C.-T., Orville, A. M., Lipscomb, J. D., Ohlendorf, D. H., and Que, L., Jr. (1992) Resonance Raman studies of the protocatechuate 3,4-dioxygenase from *Brevibacterium fuscum*, *Biochemistry 31*, 10443−10448.
26. Gaber, B. P., Sheridan, J. P., Bazer, F. W., and Roberts, R. M. (1979) Resonance Raman scattering from uteroferrin, the purple glycoprotein of the porcine uterus, *J. Biol. Chem. 254*, 8340−8342.
27. Stubbe, J., and Van der Donk, W. A. (1998) Protein radicals in enzyme catalysis, *Chem. Rev. 98*, 705−762.
28. Pesavento, R. P., and van der Donk, W. A. (2001) Tyrosyl radical cofactors, *Adv. Protein Chem. 58*, 317−385.
29. Shi, W., Hoganson, C. W., Espe, M., Bender, C. J., Babcock, G. T., Palmer, G., Kulmacz, R. J., and Tsai, A.-l. (2000) Electron paramagnetic resonance and electron nuclear double resonance spectroscopic identification and characterization of the tyrosyl radicals in prostaglandin H synthase I, *Biochemistry 39*, 4112−4121.
30. Liu, A., Pötsch, S., Davydov, A., Barra, A.-L., Rubin, H., and Gräslund, A. (1998) The tyrosyl free radical of recombinant ribonucleotide reductase from *Mycobacterium tuberculosis* is located in a rigid hydrophobic pocket, *Biochemistry 37*, 16369−16377.
31. Evelo, R. G., Styring, S., Rutherford, A. W., and Hoff, A. J. (1989) EPR relaxation measurements of photosystem II. Influence of S-state oxidation and temperature, *Biochim. Biophys. Acta 973*, 428−442.
32. Zounl, A., Witt, H.-T., Kern, J., Fromme, P., Krauss, N., Saenger, W., and Orth, P. (2001) Crystal structure of photosystem II from *Synechococcus elongatus* at 3.8 Å resolution, *Nature 409*, 739−743.
33. Dunning Hotopp, J. C., and Hausinger, R. P. (2002) Probing the 2,4-dichlorophenoxyacetate/α-ketoglutarate dioxygenase substrate binding site by site-directed mutagenesis and mechanism-based inactivation, *Biochemistry 41*, 9787−9794.
34. Ormö, M., deMaré, F., Regnström, K., Aberg, A., Sahlin, M., Ling, J., Loehr, T. M., Sanders-Loehr, J., and Sjöberg, B.-M. (1992) Engineering of the iron site in ribonucleotide reductase to a self-hydroxylating monooxygenase, *J. Biol. Chem. 267*, 8711−8714.
35. Sono, M., Roach, M. P., Coulter, E. D., and Dawson, J. H. (1996) Heme-containing oxygenases, *Chem. Rev. 96*, 2841−2887.
36. Wallar, B. J., and Lipscomb, J. D. (1996) Dioxygen activation by enzymes containing binuclear non-heme iron clusters, *Chem. Rev. 96*, 2625−2657.
37. Counts, D. F., Cardinale, G. J., and Udenfriend, S. (1978) Prolyl hydroxylase half reaction: peptidyl prolyl-independent decarboxylation of α-ketoglutarate, *Proc. Natl. Acad. Sci. U.S.A. 75*, 2145−2149.
38. Rao, N. V., and Adams, E. (1978) Partial reaction of prolyl hydroxylase. $(Gly\text{-}Gly\text{-}Pro)_n$ stimulates α-ketoglutarate decarboxylation without prolyl hydroxylase, *J. Biol. Chem. 253*, 6327−6330.
39. Holme, E., and Lindstedt, S. (1982) Studies on the partial reaction of thymine 7-hydroxylase in the presence of 5-fluorouracil, *Biochim. Biophys. Acta 704*, 278−283.
40. Myllylä, R., Majamaa, K., Günzler, V., Hanauske-Abel, H. N., and Kivirikko, K. I. (1984) Ascorbate is consumed stoichiometrically in the uncoupled reactions catalyzed by prolyl 4-hydroxylase and lysyl hydroxylase, *J. Biol. Chem. 259*, 5403−5405.
41. Zhang, Z., Barlow, J. N., Baldwin, J. E., and Schofield, C. J. (1997) Metal-catalyzed oxidation and mutagenesis studies on the iron(II) binding site of 1-aminocyclopropane-1-carboxylate oxidase, *Biochemistry 36*, 15999−16007.
42. Logan, D. T., deMaré, F., Persson, B. O., Slaby, A., Sjöberg, B.-M., and Nordlund, P. (1998) Crystal structures of two self-hydroxylating ribonucleotide reductase protein R2 mutants: structural basis for the oxygen-insertion step of hydroxylation reactions catalyzed by diiron proteins, *Biochemistry 37*, 10798−10807.

BI026832M